

pubs.acs.org/JACS Article

Collision-Induced Unfolding Reveals Disease-Associated Stability Shifts in Mitochondrial Transfer Ribonucleic Acids

Anna G. Anders, Elizabeth D. Tidwell, Varun V. Gadkari, Markos Koutmos, and Brandon T. Ruotolo*



Cite This: J. Am. Chem. Soc. 2024, 146, 4412-4420



Read Online

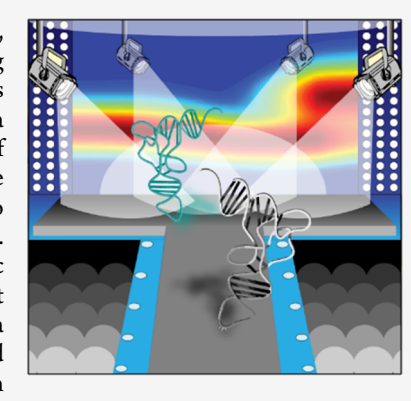
ACCESS I

Metrics & More

Article Recommendations

Supporting Information

ABSTRACT: Ribonucleic acids (RNAs) remain challenging targets for structural biology, creating barriers to understanding their vast functions in cellular biology and fully realizing their applications in biotechnology. The inherent dynamism of RNAs creates numerous obstacles in capturing their biologically relevant higher-order structures (HOSs), and as a result, many RNA functions remain unknown. In this study, we describe the development of native ion mobility-mass spectrometry and collision-induced unfolding (CIU) for the structural characterization of a variety of RNAs. We evaluate the ability of these techniques to preserve native structural features in the gas phase across a wide range of functional RNAs. Finally, we apply these tools to study the elusive mitochondrial encephalopathy, lactic acidosis, and stroke-like episodes-associated A3243G mutation. Our data demonstrate that our experimentally determined conditions preserve some solution-state memory of RNAs via the correlated complexity of CIU fingerprints and RNA HOS, the observation of predicted stability shifts in the control RNA samples, and the retention of predicted magnesium



binding events in gas-phase RNA ions. Significant differences in collision cross section and stability are observed as a function of the A3243G mutation across a subset of the mitochondrial tRNA maturation pathway. We conclude by discussing the potential application of CIU for the development of RNA-based biotherapeutics and, more broadly, transcriptomic characterization.

■ INTRODUCTION

It was not until the completion of the Human Genome Project (HGP) that the breadth of ribonucleic acid (RNA) species and their respective functions began to be realized.¹⁻³ To the surprise of many, most of the human genome did not encode for proteins but rather for RNAs that carry out key biological functions or possess unknown roles in cellular biochemistry. Since this discovery, a surge in RNA structural biology has followed, and the utility this molecular class possesses in biotherapeutic development continues to expand. 4,5 These studies have brought to light the wide range of RNA sequence lengths and types, the extensive post-transcriptional modifications (PTMs) required for their native structures and functions, the structural dynamism inherent to these biomolecules, and the manner in which both their structures and functions depend upon specific solution conditions.^{6–9} However, many of the biophysical techniques utilized for these aforementioned studies require copious amounts of sample, extensive preparation, and long analysis times and often sacrifice the native dynamism of the RNA species probed.

These challenges demand the development of new technologies capable of studying the higher-order structures (HOSs) of these noncoding RNAs (ncRNAs) both at biologically relevant concentrations and under biologically relevant solution conditions. Recently, ion mobility-mass spectrometry (IM-MS) has emerged as a useful structural biology tool, and its application to nucleic acids continues to show great promise. 1,10-13 In short, IM works by separating gas-phase ions by charge and rotationally averaged collision cross sections (CCSs) within milliseconds. 14 In conjunction with MS, ions of the same mass-to-charge (m/z) ratio and different CCSs can be readily distinguished. Importantly for RNA, extensive structural dynamics does not restrict IM-MS measurements, enabling the inherent dynamism of these biomolecules to be probed directly.

Collision-induced unfolding (CIU) has further enabled IM-MS to synchronously monitor analyte structures and stabilities¹⁵ while providing domain-level structural insight. 16,17 Specifically, CIU experiments work by collisionally activating ions of interest to induce structural unfolding prior to IM separation. In the context of protein characterization, CIU has proven powerful in discriminating differences in disulfide-bond patterns of monoclonal antibodies, classifying kinase inhibitors, and capturing RNA binding protein (RNP) substrate dependencies. 18-20 However, the utility of CIU in probing nucleic acid structures remains unexplored.

In this report, we have improved the capability of IM-MS and CIU to capture native-like gas-phase nucleic acid ions

Received: August 24, 2023 Revised: January 24, 2024 Accepted: January 25, 2024 Published: February 8, 2024





across a range of structured ncRNAs. Specifically, we experimentally determined conditions to mitigate their gasphase collapse during desolvation and better preserve nativelike Mg-bound states into the gas phase. Furthermore, we construct a series of control experiments to probe the correlations between expected shifts in RNA stability in solution and those observed by CIU and observe strong relationships between the two overall. Our optimal conditions were applied to a mitochondrial tRNA (mt-tRNA) to robustly characterize its HOS through CCS and stability measurements recorded across mt-tRNA maturation and mutation states using CIU, for the first time. Our results both confirm prior measurements obtained from previous reports and add key information pertaining to yet unprobed maturation states of the MELAS mt-tRNA leucine (Leu, UUR). Specifically, we observe that the A3243G MELAS mutation confers a significant increase in CCS in immature pre-tRNAs containing the 5'leader sequence while producing more compact configurations across other tRNA states studied, suggesting a uniquely aberrant tertiary structure is adopted for A3243G sequences prior to RNase P processing. Furthermore, we observe that the greatest degree of destabilization conferred by A3243G mutation is associated with intermediately processed tRNAs states, suggesting an uneven risk of MELAS tRNAs adopting non-native folds throughout post-transcriptional processing. We conclude our report by discussing the implications of both CIU technologies for the study of RNA structure and function, as well as the potential importance of our MELAS mt-tRNA Leu(UUR) findings.

■ EXPERIMENTAL SECTION

Sample Preparation. Solid-phase synthesized wild type (WT) and A3243G mutant mt-tRNA were purchased from Integrated DNA Technologies (IDT) and supplied as a lyophilized powder. All purchased RNAs were reconstituted using Milli-Q water (Millipore), aliquoted at 30 μ L 18 uM stocks, and stored at -80 °C. The flavin mononucleotide riboswitch aptamer (FMNRS) was in vitro transcribed (IVT) using recombinant T7 RNA polymerase and a DNA oligonucleotide template ordered from IDT (Table S3).²¹ RNA was transcribed from single-stranded antisense DNA templates containing two 5' O-methyl modifications annealed to a short complementary T7 promoter oligo.²² Transcriptions were carried out at 37 °C with orbital shaking at 300 rpm in 40 mM Tris base pH 7.9, 2 mM spermidine, 0.01% (v/v) Triton-X 100, 30 mM MgCl $_2$, 10 mM DTT, 7.11 mM ATP, 7.70 mM CTP, 10.07 mM GTP, 7.11 mM UTP, 3% (v/v) DMSO, 0.7 µM T7 RNA polymerase, 0.5 U/mL inorganic pyrophosphatase (Thermo Fisher Scientific), and 0.1 µM DNA template containing the T7 promoter sequence. After 3.75-4 h, reactions were quenched with EDTA and brought to pH at a final concentration of 60 mM. The resulting RNA was analyzed for quality and homogeneity using 12% (v/v) poly(acrylamide gel electrophoresis) (PAGE) followed by either UV back shadowing²³ or staining using methylene blue.²⁴ The transcription reactions, if sufficiently homogeneous, were further purified by size exclusion chromatography (SEC) to remove free nucleotides, short transcription termination products, and T7 RNA polymerase. Transcription mix was buffer-exchanged into denaturing SEC buffer (0.1 M Tris pH 7, 0.1 M boric acid, 0.2 mM EDTA, 5 M urea) using an Amicon spin column (30 kDa MWCO). Concentrated RNA was injected on to an equilibrated Superdex S200 15/300 column (GE Healthcare, now Cytiva) and eluted at a flow rate of 0.35 mL per minute. Using the ultraviolet (UV) chromatogram and PAGE analysis, the most homogeneous fractions were pooled and bufferexchanged using a fresh Amicon spin column (30 kDa MWCO) into a storage buffer, either TBE or 50 mM Tris, 50 mM borate, 150 mM

KCl, and aliquoted from 30 to 60 uL and flash-frozen in liquid nitrogen before storage at $-80~^{\circ}$ C.

For MS analysis, all RNAs were diluted to a working concentration of 2 μ M in 60 μ L. RNAs were thawed on ice before refolding via thermal denaturation at 90 °C for 3 min followed by incubation at 37 °C in the presence of 0.5 mM Mg(OAc)₂ for 15 min, then cooled at room temperature for 10 min before transferring to ice. For Mg²⁺-dependent folding experiments, concentrations of 0.05–20 mM Mg(OAc)₂ were used in place of 0.5 mM Mg(OAc)₂ solution referenced above. To remove nonspecifically bound Mg²⁺ ions, the folded RNAs were buffer-exchanged into pH ~7100 mM AmOAc with Micro Biospin $P\bar{6}$ Micro columns (Bio-Rad, Hercules, CA) prior to both native MS or IM-MS analyses. The modified single-stranded short interfering RNA (siRNA) and siRNA Duplex (each 60 μ L at 2 μ M) were provided by Amgen (sequences are proprietary to Amgen) and did not undergo any refolding as described above.

High-Resolution Native Mass Spectrometry. A Thermo Fisher Q-Exactive Ultra high mass resolution (QE-UHMR) Hybrid Quadrupole-Orbitrap Mass Spectrometer was used for identifying Mg-bound populations of mt-tRNA^{Leu(UUR)} identified under a negative ionization polarity. Samples were buffer-exchanged into 100 mM ammonium acetate (AmOAc) using Micro Bio-Spin P6 gel columns (Bio-Rad, Hercules, CA) and directly infused via nanoelectrospray ionization (nESI).²⁵ nESI was performed using borosilicate needles pulled and gold-coated in-house with a Sutter p-97 Needle Puller and a Quorum SCX7620 mini sputter coater, respectively. QE-UHMR acquisition settings can be found in Supporting Table 1. The acquired native mass spectra were deconvoluted using UniDec in negative polarity.²⁶

IM-MS and CIU. An Agilent 6560C (Agilent Technologies, Santa Clara, CA) was utilized for all IM-MS and CIU experiments where the instrument configuration has been previously described. ^{27,28} RNA samples were subjected to nESI (capillary voltages of 1.2–1.5 kV) with in-house pulled borosilicate capillary needles. For higher insource activation (>390 V), sulfur hexafluoride (SF₆) was used as a drying gas between the fragmentor (F) and capillary exit (CE) lenses to act as an electron scavenger and prevent arcing. Additionally, SF₆(g) has a larger mass than the typical N_2 gas used in this region of the instrument and results in higher center-of-mass-frame kinetic energy collisions with the analyte ions. Throughout the rest of the instrument, high-purity nitrogen $(N_{2(g)})$ was used. Additional 6560C settings can be found in the Supporting Information (Table S2).

Multifield CCS measurements were conducted across 1450–1700 V (by 50 V increments) at the drift tube entrance voltage and collected in 0.5 min intervals. CIU experiments were conducted by increasing the CE lens (up to +490 V) relative to the F lens (400 V). Specifically, 10 V steps at 0.2 min were acquired from 10 to 480 V CE. The time segment feature was used in the Agilent Mass Hunter 10 Acquisition software to collect all activation steps in a single file. The MIDAC Agilent data extractor (packaged with CIUSuite2) was used to extract the arrival time distributions (ATDs) for the ions of interest from each time segment. The ATDs were plotted against the applied $\Delta V_{\rm r}$ referred to as collision voltage (CV), using CIUSuite2.3. Importantly, this version of CIUSuite2 29 is crucial for accurate fitting of the compaction transition observed in nucleic acid CIU.

CIU Data Processing. β -version CIUSuite2.3 was used for the CIU analysis of all nucleic acids (Figure S1). Specifically, raw instrument files were loaded via CIU batch extraction to generate .raw files. Within the batch extraction template, upper and lower m/z values were specified by charge state, and t0 (t-fix) and β (β) values were provided. t0 and β were acquired by spraying Agilent tunemix in a negative ionization polarity. The resulting mass spectra were subsequently analyzed in IM-MS Browser 10, and the single-field CCS calculator was used to extract the drift times of each tunemix ion to obtain t0 (t-fix) and β (β) values for CIU-CCS calibration. Additionally, high energy and non-time-segmented (a value of "0") was specified for the extraction.

Resulting text _raw.csv files were then used as input for CIUSuite2 data processing, using a smoothing window size of 5 and 1 iteration (2D Savitzky-Golay). The data were interpolated by a factor of 2 and cropped in both axes to better visualize the resulting fingerprint. Data

were plotted and underwent standard feature detection with the "exclude feature" set to false for all CIU50 analyses reported here.

RESULTS AND DISCUSSION

Ribonucleic Acids Structurally Compact prior to Unfolding. Prior reports have detailed the potential of CIU assays to probe the structures and stabilities of a variety of proteins and protein complexes. Typical CIU experiments produce increased drift times or CCSs in a manner correlated with increases in collision voltage (CV), with some cavity-containing protein complexes observed to undergo compaction upon collisional activation. Prior to this report, CIU has not been used to study the HOS of RNA species, and a key objective of the studies described here centered on evaluating the information content of such assays applied to nucleic acid targets.

We selected three RNA species of varying HOS (e.g., primary, secondary, tertiary) and hypothesized that their resulting CIU fingerprints would reflect patterns indicative of their differences in HOS as RNAs with more complex secondary and tertiary structures were probed. Pilot CIU experiments focused on an siRNA, a double-stranded RNA duplex, and a mt-tRNA. Our CIU data revealed that both the number of CIU features and the CIU50 values recorded depend strongly on RNA HOS (Figure 1). In contrast to the majority of protein CIU, RNA ions routinely undergo an initial compaction step upon collisional activation prior to CIU to a variable extent. However, when evaluated across ionization polarities, charge states, ion species, and levels of pre-CIU HOS, this compaction remains the most prominent aspect of RNA CIU data sets (Figures S2 and S3). MS evaluation across respective CIU features reveals there to be no change in RNA mass during compaction (e.g., no loss of RNA bases), thus suggesting that an alteration in RNA HOS is the most likely origin of the observed shift in RNA CCS values (Figure S4).

Prior experiments have observed the compaction of large biomolecules upon desolvation during ESI, including nucleic acids. ^{31–37} A closer analogue to the collision-initiated RNA compaction observed in our RNA CIU data includes the compaction steps observed for cavity-containing multiprotein complex ions during CIU, where such transitions have been linked to the collapse of such cavity-bearing structures as a low-energy remodeling pathway during the collisional activation of such ions in the gas phase. ³⁰ Despite such similarities, it is not possible currently to draw direct comparisons between our RNA CIU data and these prior reports due to the differing polarities, chemical compositions, and potential for salt-bridged structures within the two ion classes.

IM-MS Preserves Native-like Mg²⁺-Ensemble Populations into the Gas Phase. As noted above, previous native MS work on nucleic acids has revealed that such ion species undergo significant gas-phase collapse upon desolvation during ESI.^{38,39} While the findings outlined above could suggest a loss of native-like structure upon desolvation, it has also been observed that nucleic acids can retain their specific cofactor and ligand interactions from the solution during MS analyses (Figure S7).^{40–45} Prior reports in this area have focused primarily on characterizing either rigid nucleic acid structures or nucleic acid forms produced in the absence of biologically relevant cationic cofactors (e.g., Mg²⁺, Na⁺, K⁺) due to the incompatibility of high salt concentrations with ESI. As such, the overall level of native higher-order structural information

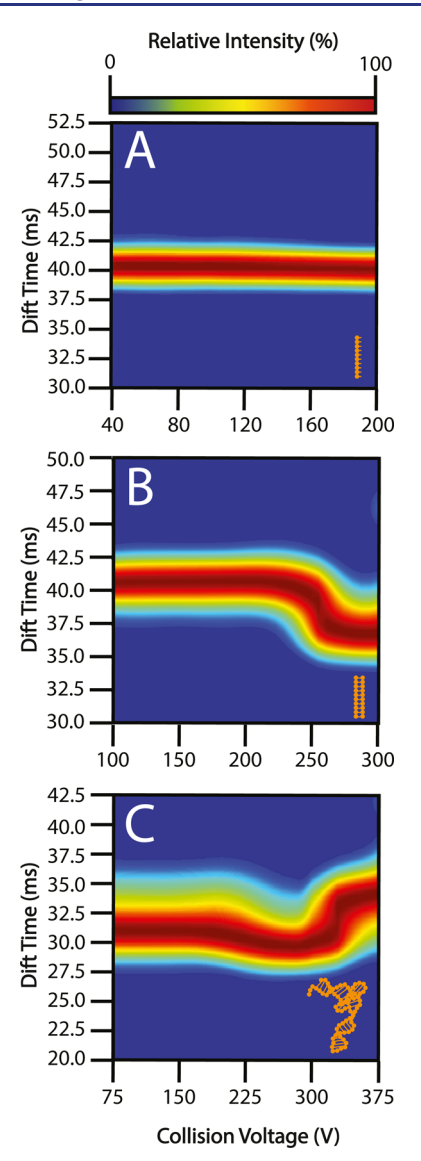


Figure 1. CIU detects HOSs in RNA species. Top to bottom (A–C), RNA species increase in their higher-order structural complexity. (A) A single-stranded short interfering RNA (siRNA) of primary structure. (B) An RNA duplex of secondary structure. (C) A mt-tRNA of tertiary structure. CIU analyses support the expected increase in HOS through the observed increasing number of features observed ($n \ge 3$, RMSDs ≤ 2.00 for all).

preserved in the gas phase for less rigid nucleic acid structures remains largely unknown.

We began recreating these previous experiments, and we further explored other reported solution conditions to discover which would adequately stabilize native-like RNA structures for IM-MS characterization. Ultimately, we found that solutions containing 100 mM AmOAc when ionized in negative polarity mode were optimal for the IM-MS analyses of flexible RNAs. The ionic strength identified in our survey is lower than the optimal value reported previously for rigid nucleic acid species, ¹³ yet it was chosen for its ability to promote more native-like CCSs values in the RNA species studied here while preserving a native charge state envelope (i.e., low charge states indicative of folded RNA structures). The negative ionization polarity was selected for its ability to confer improved signal intensities for RNA species due to their

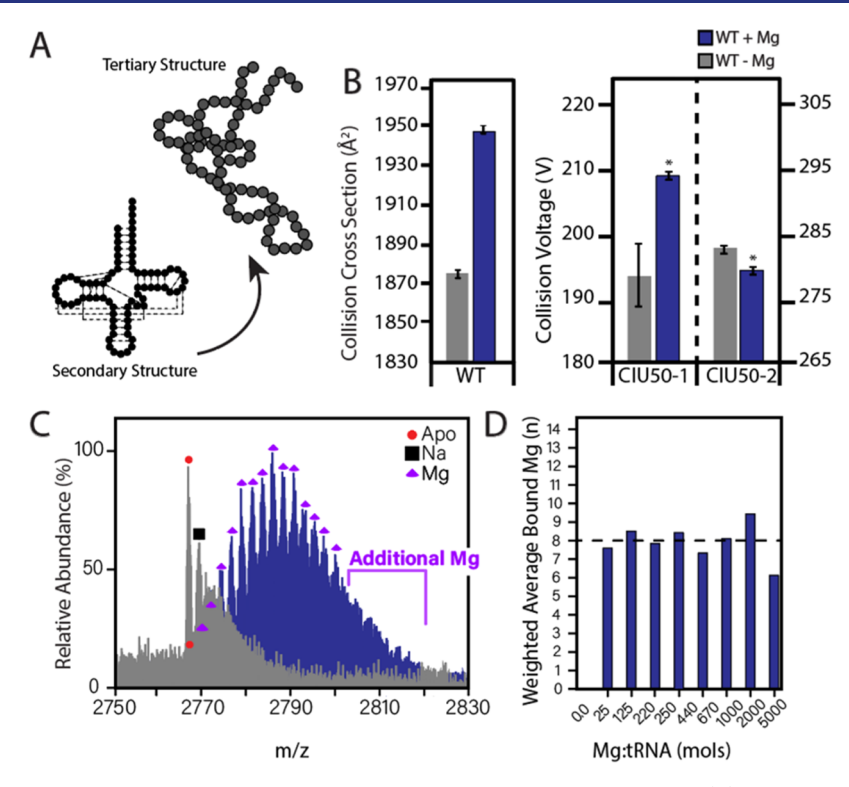


Figure 2. (A) tRNA secondary structure with predicted contacts to adopt the final tertiary structure. (B) Centroid fitted CCS and CIU50 Mg^{2+} dependences of the WT mt-tRNA^{Leu(UUR)} species ($n \ge 3$, $p \le 0.01$). (C) Native mass spectra of the Mg^{2+} -free 3'CCA species (gray) and a common Mg^{2+} folding concentration (blue). Metal-free tRNAs are denoted by red circles, sodium by black squares, and Mg^{2+} by purple triangles. (D) Weighted averages of Mg^{2+} :tRNA as a function of $Mg(OAc)_2$ concentration ($n \ge 3$). It is important to note that all Mg^{2+} peaks across each $Mg(OAc)_2$ concentration were accounted for in the weighted average calculation.

greater anionic ionization efficiencies (Figure S5A) and for the preservation of a native-net overall charge for RNA species, which can be a concern for the evaluation of biomolecular HOS, when compared to equivalent positive polarity data sets (Figures S5 and S6).

In addition to the considerations detailed above, various magnesium (Mg²⁺) concentrations were explored in our evaluation of solution conditions designed to preserve nativelike RNA HOS for IM-MS investigations. Mg²⁺ is a particularly important cofactor required for RNA structure, function, catalysis, and RNA binding proteins (RBPs).46-48 In the context of RNA folding, Mg²⁺ concentrations vary extensively in solution-based folding protocols and commonly use magnesium chloride (MgCl $_2$). Because free chloride (Cl $^-$) ions can lead to ion suppression in ESI, a Mg(OAc)2 salt was chosen as a source of Mg²⁺ ions and for its MS-compatible counterion (acetate, OAc⁻). Preliminary data collection was aimed at identifying if the solution structural Mg²⁺ effects were retained in the gas phase using a highly structured flavin mononucleotide riboswitch (FMNRS) aptamer (Figure S8). 50 Upon the addition of micromolar amounts of Mg(OAc), to RNA samples in solution, significant changes in both the RNA CCS and stability were observed in our IM-MS data. Mg²⁺induced stabilization in RNA structures has been well reported in prior studies⁵¹⁻⁵⁴ and is reflected in CIU50 values that increase in a manner correlated with increasing Mg(OAc), concentrations. However, given the nonlinear nature of the correlation observed, we focused our efforts on determining the optimal amount of Mg(OAc)₂ for IM-MS and CIU characterization of structured and flexible RNA targets.

To identify optimal Mg²⁺ concentrations for native IM-MS studies of less rigid nucleic acid structures, an mt-tRNA (specifically, mt-tRNA^{Leu(UUR)}) was used as a model system. Overall, tRNAs often serve as model RNA systems due to their well-characterized solution-states, canonical secondary and tertiary structures (Figures 2A and S9),^{55–58} and discrete structural dependence on Mg²⁺ binding.⁵⁵ mt-tRNAs serve as unique tRNA species due to their hypothesized increase in dynamism when compared to cytosolic tRNAs.^{58,59} Despite this increased dynamism, current literature identifies the presence of eight specifically bound Mg²⁺ ions for natively structured tRNAs,⁵⁸ and we have utilized native MS to determine if this stoichiometry is preserved within the tRNA ion-ensembles detected in the gas phase.

Specifically, the canonically elbow-shaped, mature 3'CCAcontaining wild-type synthesized mitochondrial (mt)-tRNA Leucine (LEU, UUR) was folded in concentrations of Mg(OAc)₂ ranging from 0.05 to 20 mM in 100 mM AmOAc (Figure S17, not all concentrations tested shown). As observed in our FMNRS data, we detect a stabilization and a change in CCS upon the addition of Mg(OAc)2 to mt $tRNA^{Leu(UUR)}$ samples (Figure 2B). These data comport with the conclusion that shifts in the compaction step observed in our data, quantified by CIU50-1, contain biomolecular stability information that strongly correlates with expected shifts in solution. Specifically, we observe a dramatic increase in CIUbased stability upon folding the tRNA in the presence of Mg when compared to RNA that has not been subjected to proper RNA folding conditions. Control experiments verified that shifts in CIU50 are not due to the addition of Mg alone (Figure S10). These data align with further control experiments where we observe increases in RNA stability upon the addition of post-transcriptional modifications known to stabilize the tRNA structure (Figure S14) and upon RNA-ligand binding (Figure S7). Taken together, these data strongly indicate that the RNA stability information extracted from CIU is strongly correlated with relative shifts associated with RNA stability in solution.

Our native MS data identify a plethora of Mg²⁺:tRNA stoichiometries under the above-noted solution conditions, and as expected, with increasing Mg²⁺ concentrations in solution, we detect an increase in Mg²⁺-binding/adduction to the RNA ions observed in our experiments. Despite this, we note that the weighted average of all Mg-bound RNA ion populations observed across all Mg concentrations greater than $\sim\!75~\mu\mathrm{M}$ (a 25-fold excess relative to our tRNA concentration) produced values of 8 \pm 1 Mg²⁺ ions bound (Figure 2C), with larger Mg²⁺-binding stoichiometries observed with insufficient intensity to significantly shift this average at higher Mg²⁺ concentrations.

While our native MS experiments were able to detect the predicted Mg^{2+} -RNA stoichiometry for the properly folded mt- $tRNA^{Leu(UUR)}$, it is important to note that we anticipated detecting an ensemble of Mg²⁺-binding states in our native MS RNA measurements due, in part, to the structural dynamism and polydispersity inherent to such biomolecules. In addition, it is important to note that there are two types of Mg²⁺-RNA interactions expected in our data: site-specific tightly bound Mg²⁺ ions and those that are associated with a secondary solvation shell primarily serving as counterions. Taken together, our experiments have likely captured Mg²⁺ ions mainly belonging to the former category alongside a subset of the latter category of bound Mg2+. Aside from Mg2+, it is important to note that cations such as sodium (Na+) and potassium (K⁺) are abundant within living cells and have been shown to be involved in several nucleic acid structures. Specifically, tRNAs have been identified to utilize Na⁺ in addition to Mg²⁺, and future work aims to address the concentrations of such ions needed for the improved analysis of native-like tRNAs in the absence of bulk solvent.

Shifts in MELAS-Associated tRNA Structure and Stability. Human mitochondria are unique in that they contain their own genome and encode for a complete set of tRNAs separate from cytosolic tRNAs. Importantly, these mt-tRNAs incur significant rates of mutation due to the highly oxidative environment native to the mitochondria, and these mutations result in several mitochondrial disorders that remain difficult to capture and characterize. Mitochondrial encephalopathy, lactic acidosis, and stroke-like episodes (MELAS) remain one of the most common, and often fatal, mitochondrial disorders beginning in early childhood, affecting both the nervous and muscular systems. In approximately 80% of cases, an A3243G transition mutation occurring in the mt-tRNA Leu(UUR) is observed and correlated to the onset of the disorder. While the current consensus is that this mutation negatively affects mitochondrial translation, the biophysical consequences of this mutation remain poorly understood.

Like cytosolic tRNAs, mt-tRNAs undergo 5' and 3' end processing, but these processing points differ in that mt-tRNAs are cleaved via the tRNA punctuation model unlike their cytosolic counterparts (Figure S11).⁶⁰ Currently, most prior work focusing on the A3243G MELAS RNA mutation has surrounded its ability to be processed by mitochondrial ribonuclease P (mt-RNase P) at the 5'leader sequence,^{66,67}

but the effects the mutation induces across mt-tRNA maturation states have remained unexplored until now. Specifically, we leveraged the optimal solution and instrument conditions identified in the data described above for native-like gas-phase RNA analyses to probe the biophysical consequences this mutation induces onto the mt-tRNAs across a subset of the RNA maturation pathway (Figure 3A).

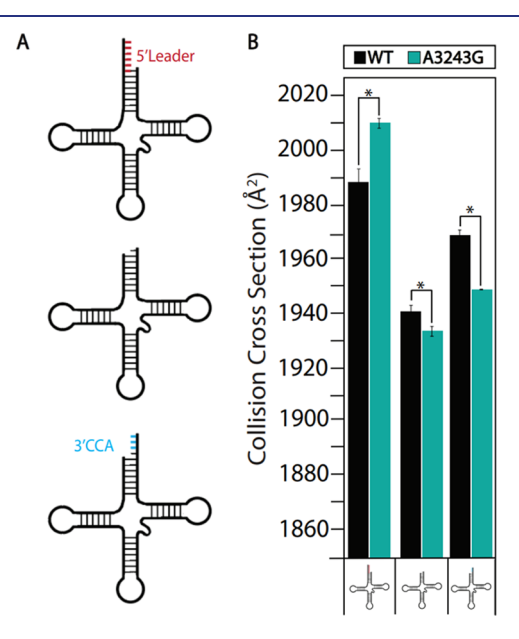


Figure 3. (A) Simplified mt-tRNA structures. Specifically, a 5'leader-containing species (red), mature mt-tRNA, and a 3'CCA species (blue) were characterized in this work. It is important to note that following 3'CCA addition, these species are post-transcriptionally modified for mature functioning. (B) Centroid fitted CCSs of the WT (black) and A3243G (turquoise) mt-tRNA^{Leu(UUR)} across the maturation pathway (z8 $^-$, n=5, $p\leq0.005$). Significant differences in the CCS are observed across the mutation and the respective maturation species.

In agreement with previous A3243G mutant results, an increase in RNA dimerization is observed for the 3'CCA-containing species (Figure S12),⁶⁸ and for the first time, our data show an increase in dimerization for the 5'leadercontaining species (Figure S12). Overall, CCS data reveal significant differences across each point of maturation and mutation, but the effects of these structural changes induced in the specific RNA species studied are difficult to interpret through CCS information alone (Figure 4A). If the structure of the mt-tRNA remains unchanged, the reduced mass associated with the A3243G mutation alone is likely to be insufficient to shift the observed CCS of the intact mt-tRNA. Interestingly, we note that these changes in mt-tRNA CCS were not observed in the absence of Mg²⁺. As such, while our CCS data indicates changes in mt-tRNA structure upon A3243G mutation, such data alone does not allow us to draw distinct conclusions regarding the nature of the RNA HOS alterations produced.

In our CIU data, we reveal differences between mt-tRNA variants (Figure S13). Specifically, we observe that the A3243G mutation significantly destabilizes each mt-tRNA maturation state (Figure 4B). Likely, this destabilization stems from a hypothesized disruption of a conserved D-T loop interaction, an essential interaction for the adoption of the proper tertiary structure (Figure S9). Taken together, the CCS

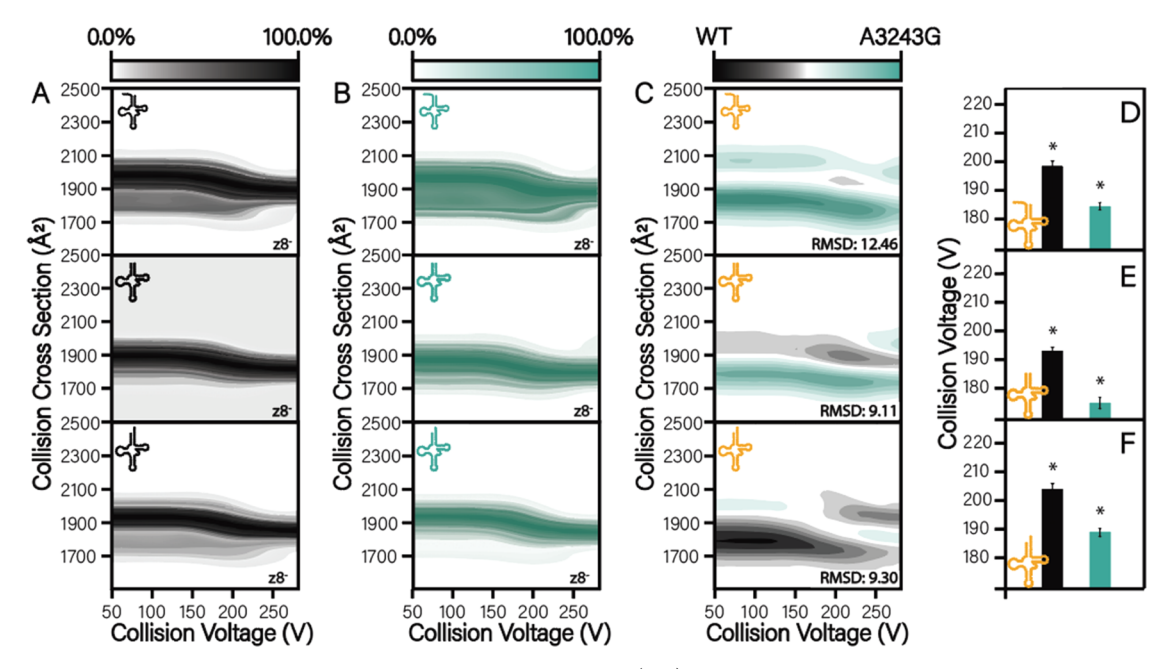


Figure 4. (A) Average CIU fingerprints of the WT (black) of mt-tRNA^{Leu(UUR)} in order of maturation (top to bottom). (B) Average CIU fingerprints of the A3243G mutant (teal) in order of maturation (top to bottom). (C) Average CIU fingerprint comparisons between the WT and A3243G species. (D−F) Compaction (CIU50-1) of the WT and A3243G mutant across maturation (top to bottom) ($n \ge 5$ for all, replicate RMSDs ≤ 2.00, $p \le 0.01$).

and CIU data indicate a topological disruption in the mt-tRNA HOS in the A3243G mutant. Furthermore, when combined with data shown in Figure 2, we theorize that CIU50-1 can perhaps be attributed to the collapse of RNA tertiary structure elements associated with Mg-binding (Figure S9). 54,56

Interestingly, when our WT mt-tRNA IM-MS data are examined closely, unique trends are observed across the maturation pathway. While the CCSs appear to be related to the overall mt-tRNA sequence length (where an increase in length likely relates to an increase in size), the trends in stability are more difficult to rationalize. The final addition of the 3'CCA confers greater stability than the longer 5'leader sequence, while the species lacking both a 5'leader and 3'CCS is the most unstable. It is likely that specific nucleotides are contributing to the observed trends in RNA stability (e.g., canonical base pairing between the sixth nucleotide of the 5'leader with the 75th base of the 5'leader-containing species), and future work investigating single-nucleotide truncations is needed to identify how these nucleotides affect the structure of each species. Finally, mt-tRNAs are highly dependent upon post-transcriptional modifications (PTMs) for proper structure and function (Figure S16). 67,-70 The species in this work were produced using solid-phase synthesis; thus, additional work exploring the post-transcriptionally modified maturation structures and the A3243G mutation is needed.

CONCLUSIONS

In this study, we have extensively characterized the utility of IM-MS and CIU to probe the HOS of large, dynamic nucleic acids. For the first time, CIU was utilized to probe RNA HOS, and our results indicate an overall increase in CIU fingerprint complexity as the number of discrete HOS elements is added to the structures of the RNAs analyzed. Additionally, CIU50 analyses recapitulate RNA stabilization and structural dependence on its folded status in the presence of Mg²⁺. Across each set of conditions tested, our results further demonstrate a well-

conserved structural compaction prior to unfolding in RNAs. While the overall level of compaction was found to be dependent upon RNA HOS, charge state, ion polarity, and solution conditions, it is potentially a feature common to all RNA CIU data.

In a more general sense, a set of conditions for the native IM-MS analysis of nonrigid RNAs were identified where these conditions proved to preserve Mg2+ specificity and ligand binding (i.e., FMN to the FMNRS) while mitigating gas-phase collapse typically observed following ESI. This gas-phase collapse was mitigated through a systemic identification of optimal solution conditions in terms of ionic strength and counterion concentrations. In agreement with previous work, an increase in CCS is observed with decreasing ionic strength in solution, and 100 mM AmOAc was ultimately chosen as it produced the most native-like CCS values without altering the native charge envelope of the RNA ions produced. These conditions were applied to a well-studied tRNA and ultimately observed to preserve specific bound states of the Mg²⁺ cofactor for the mt-tRNA Leu(UUR) species. Taken together, these conditions permitted evaluation of the A3243G mttRNA^{Leu(UUR)} mutation, allowing us to quantify significant topological and stability differences across the mt-tRNA maturation pathway for this disease-associated nucleic acid.

Finally, these results indicate that some native-like properties of RNA HOSs are preserved in the gas phase. Our control CIU experiments with mt-tRNA^{Leu(UUR)}, the FMNRS, and tRNA^{Ser(GCU)} revealed expected shifts in RNA stability across the PTM status, ligand binding, the use of proper RNA folding procedures, and maturation level. As such, our data strongly indicates that CIU stability information is correlated to the biophysical properties of RNA in solution. Future research will be focused on the deployment of CIU to probe specific RNA secondary structures (e.g., hairpins, internal loops, pseudoknots, etc.) which could provide an informative roadmap for CIU fingerprint-interpretation. Future efforts

involving the characterization of RNA compaction during CIU through a combination of solution, MS, and computational studies may provide new information surrounding RNA structure and polyanionic gas-phase species, in general.

ASSOCIATED CONTENT

Supporting Information

The Supporting Information is available free of charge at https://pubs.acs.org/doi/10.1021/jacs.3c09230.

MS, IM-MS, and CIU data containing ligand binding, RNA PTMs, buffer concentrations, mutations, and Mg²⁺-binding information; graphical representations or tables of RNA structures, mt-tRNA processing pathway, CIUSuite data processing, UHMR and 6560C instrument settings, and RNA sequences (PDF)

AUTHOR INFORMATION

Corresponding Author

Brandon T. Ruotolo — Department of Chemistry, University of Michigan, Ann Arbor, Michigan 48109, United States; orcid.org/0000-0002-6084-2328; Phone: 1-734-615-0198; Email: bruotolo@umich.edu; Fax: 1-734-615-3718

Authors

Anna G. Anders — Department of Chemistry, University of Michigan, Ann Arbor, Michigan 48109, United States

Elizabeth D. Tidwell — Department of Biophysics, University of Michigan, Ann Arbor, Michigan 48109, United States

Varun V. Gadkari — Department of Chemistry, University of Minnesota, Minneapolis, Minnesota 55455, United States;

orcid.org/0000-0001-6145-3773

Markos Koutmos — Department of Chemistry, University of Michigan, Ann Arbor, Michigan 48109, United States; Department of Biophysics, University of Michigan, Ann Arbor, Michigan 48109, United States

Complete contact information is available at: https://pubs.acs.org/10.1021/jacs.3c09230

Notes

The authors declare no competing financial interest.

ACKNOWLEDGMENTS

This work was supported by the Chemical Biology Training Program (CBTP; 5T32GM008353-30 to A.A), Agilent Technologies, the UM Biosciences Initiative, the National Institutes of Health (GM117141), and the National Science Foundation (1808541 and 2304961) Chemical Measurement and Imaging Program with partial co-funding from the Division of Molecular and Cellular Biosciences. tRNAs were provided by Dr. Joshua Jones and Prof. Kristin Koutmou in the Department of Chemistry at the University of Michigan. The authors thank Jennifer L. Lippens and Zhuoer Xie of Amgen, Inc. for helpful discussions and for providing siRNA samples.

ABBREVIATIONS

IM-MS, ion mobility—mass spectrometry; CIU, collision-induced unfolding; mt-tRNA, mitochondrial transfer ribonucleic acid; FMNRS, flavin mononucleotide riboswitch; siRNA, short interfering ribonucleic acid; MS, mass spectrometry; MELAS, mitochondrial encephalopathy, lactic acidosis, and stroke-like episodes; HOS, higher-order structure; SEC, size

exclusion chromatography; PAGE, poly(acrylamide gel electrophoresis)

REFERENCES

- (1) Nucleic Acids in the Gas Phase; Gabelica, V., Ed.; Physical Chemistry in Action; Springer: Heidelberg, 2014.
- (2) Xu, B.; Zhu, Y.; Cao, C.; Chen, H.; Jin, Q.; Li, G.; Ma, J.; Yang, S. L.; Zhao, J.; Zhu, J.; Ding, Y.; Fang, X.; Jin, Y.; Kwok, C. K.; Ren, A.; Wan, Y.; Wang, Z.; Xue, Y.; Zhang, H.; Zhang, Q. C.; Zhou, Y. Recent Advances in RNA Structurome. *Sci. China Life Sci.* 2022, 65 (7), 1285–1324, DOI: 10.1007/s11427-021-2116-2.
- (3) Xu, B.; Zhu, Y.; Cao, C.; Chen, H.; Jin, Q.; Li, G.; Ma, J.; Yang, S. L.; Zhao, J.; Zhu, J.; Ding, Y.; Fang, X.; Jin, Y.; Kwok, C. K.; Ren, A.; Wan, Y.; Wang, Z.; Xue, Y.; Zhang, H.; Zhang, Q. C.; Zhou, Y. Recent Advances in RNA Structurome. *Sci. China Life Sci.* **2022**, *65* (7), 1285–1324, DOI: 10.1007/s11427-021-2116-2.
- (4) Zhu, Y.; Zhu, L.; Wang, X.; Jin, H. RNA-Based Therapeutics: An Overview and Prospectus. *Cell Death Dis.* **2022**, *13* (7), 644 DOI: 10.1038/s41419-022-05075-2.
- (5) Spitale, R. C.; Incarnato, D. Probing the Dynamic RNA Structurome and Its Functions. *Nat. Rev. Genet.* **2023**, 24 (3), 178–196
- (6) Ontiveros, R. J.; Stoute, J.; Liu, K. F. The Chemical Diversity of RNA Modifications. *Biochem. J.* **2019**, 476 (8), 1227–1245.
- (7) Ganser, L. R.; Kelly, M. L.; Herschlag, D.; Al-Hashimi, H. M. The Roles of Structural Dynamics in the Cellular Functions of RNAs. *Nat. Rev. Mol. Cell Biol.* **2019**, 20 (8), 474–489.
- (8) Dai, X.; Zhang, S.; Zaleta-Rivera, K. RNA: Interactions Drive Functionalities. *Mol. Biol. Rep.* **2020**, *47* (2), 1413–1434.
- (9) Wang, X.-W.; Liu, C.-X.; Chen, L.-L.; Zhang, Q. C. RNA Structure Probing Uncovers RNA Structure-Dependent Biological Functions. *Nat. Chem. Biol.* **2021**, *17* (7), 755–766.
- (10) Zhong, Y.; Hyung, S.-J.; Ruotolo, B. T. Ion Mobility—Mass Spectrometry for Structural Proteomics. *Expert Rev. Proteomics* **2012**, 9 (1), 47–58, DOI: 10.1586/epr.11.75.
- (11) Fabris, D.Ion Mobility—Mass Spectrometry of Nucleic Acids. In *Ion Mobility-Mass Spectrometry*, New Developments in Mass Spectrometry; The Royal Society of Chemistry, 2021; pp 461–495.
- (12) Kenderdine, T.; Fabris, D. The Multifaceted Roles of Mass Spectrometric Analysis in Nucleic Acids Drug Discovery and Development. *Mass Spectrom. Rev.* **2023**, 42, 1332–1357, DOI: 10.1002/mas.21766.
- (13) Largy, E.; König, A.; Ghosh, A.; Ghosh, D.; Benabou, S.; Rosu, F.; Gabelica, V. Mass Spectrometry of Nucleic Acid Noncovalent Complexes. *Chem. Rev.* **2022**, *122* (8), 7720–7839.
- (14) Ruotolo, B. T.; Benesch, J. L. P.; Sandercock, A. M.; Hyung, S.-J.; Robinson, C. V. Ion Mobility–Mass Spectrometry Analysis of Large Protein Complexes. *Nat. Protoc.* **2008**, *3* (7), 1139–1152.
- (15) Dixit, S. M.; Polasky, D. A.; Ruotolo, B. T. Collision Induced Unfolding of Isolated Proteins in the Gas Phase: Past, Present, and Future. *Curr. Opin. Chem. Biol.* **2018**, 42, 93–100.
- (16) Eschweiler, J. D.; Martini, R. M.; Ruotolo, B. T. Chemical Probes and Engineered Constructs Reveal a Detailed Unfolding Mechanism for a Solvent-Free Multidomain Protein. *J. Am. Chem. Soc.* **2017**, *139* (1), 534–540.
- (17) Zhong, Y.; Han, L.; Ruotolo, B. T. Collisional and Coulombic Unfolding of Gas-Phase Proteins: High Correlation to Their Domain Structures in Solution. *Angew. Chem.* **2014**, *126* (35), 9363–9366.
- (18) Tian, Y.; Han, L.; Buckner, A. C.; Ruotolo, B. T. Collision Induced Unfolding of Intact Antibodies: Rapid Characterization of Disulfide Bonding Patterns, Glycosylation, and Structures. *Anal. Chem.* **2015**, 87 (22), 11509–11515.
- (19) Rabuck-Gibbons, J. N.; Keating, J. E.; Ruotolo, B. T. Collision Induced Unfolding and Dissociation Differentiates ATP-Competitive from Allosteric Protein Tyrosine Kinase Inhibitors. *Int. J. Mass Spectrom.* **2018**, 427, 151–156.
- (20) Politis, A.; Park, A. Y.; Hall, Z.; Ruotolo, B. T.; Robinson, C. V. Integrative Modelling Coupled with Ion Mobility Mass Spectrometry Reveals Structural Features of the Clamp Loader in Complex with

- Single-Stranded DNA Binding Protein. *J. Mol. Biol.* **2013**, 425 (23), 4790–4801.
- (21) Serganov, A.; Huang, L.; Patel, D. J. Coenzyme Recognition and Gene Regulation by a Flavin Mononucleotide Riboswitch. *Nature* **2009**, 458 (7235), 233–237.
- (22) Milligan, J. F.; Groebe, D. R.; Witherell, G. W.; Uhlenbeck, O. C. Oligoribonucleotide synthesis using T7 RNA polymerase and synthetic DNA templates. *Nucleic Acids Res.* **1987**, *15* (21), 8783–8798, DOI: 10.1093/nar/15.21.8783.
- (23) Hendry, P.; Hannan, G. Detection and Quantitation of Unlabeled Nucleic in Polyacrylamide Gels. *Biotechniques* **1996**, 20 (2), 258–264.
- (24) Hossain, M.; Suresh Kumar, G. DNA Intercalation of Methylene Blue and Quinacrine: New Insights into Base and Sequence Specificity from Structural and Thermodynamic Studies with Polynucleotides. *Mol. Biosyst.* **2009**, *5* (11), 1311–1322.
- (25) Konermann, L.; Ahadi, E.; Rodriguez, A. D.; Vahidi, S. Unraveling the Mechanism of Electrospray Ionization. *Anal. Chem.* **2013**, 85 (1), 2–9.
- (26) Marty, M. T.; Baldwin, A. J.; Marklund, E. G.; Hochberg, G. K. A.; Benesch, J. L. P.; Robinso—n, C. V. Bayesian Deconvolution of Mass and Ion Mobility Spectra: From Binary Interactions to Polydisperse Ensembles. *Anal. Chem.* **2015**, *87* (8), 4370—4376.
- (27) Gadkari, V. V.; Ramírez, C. R.; Vallejo, D. D.; Kurulugama, R. T.; Fjeldsted, J. C.; Ruotolo, B. T. Enhanced Collision Induced Unfolding and Electron Capture Dissociation of Native-like Protein Ions. *Anal. Chem.* **2020**, *92* (23), 15489–15496.
- (28) Gadkari, V. V.; Juliano, B. R.; Mallis, C. S.; May, J. C.; Kurulugama, R. T.; Fjeldsted, J. C.; McLean, J. A.; Russell, D. H.; Ruotolo, B. T. Performance Evaluation of In-Source Ion Activation Hardware for Collision-Induced Unfolding of Proteins and Protein Complexes on a Drift Tube Ion Mobility-Mass Spectrometer. *Analyst* 2023, 148 (2), 391–401.
- (29) Polasky, D. A.; Dixit, S. M.; Fantin, S. M.; Ruotolo, B. T. CIUSuite 2: Next-Generation Software for the Analysis of Gas-Phase Protein Unfolding Data. *Anal. Chem.* **2019**, *91* (4), 3147–3155.
- (30) Hall, Z.; Politis, A.; Bush, M. F.; Smith, L. J.; Robinson, C. V. Charge-state dependent compaction and dissociation of protein complexes: Insights from Ion Mobility and molecular dynamics. *J. Am. Chem. Soc.* **2012**, *134* (7), 3429–3438.
- (31) Ruotolo, B. T.; Giles, K.; Campuzano, I.; Sandercock, A. M.; Bateman, R. H.; Robinson, C. V. Evidence for Macromolecular Protein Rings in the Absence of Bulk Water. *Science* **2005**, *310* (5754), 1658–1661.
- (32) Rolland, A. D.; Prell, J. S. Computational Insights into Compaction of Gas-Phase Protein and Protein Complex Ions in Native Ion Mobility-Mass Spectrometry. *TrAC, Trends Anal. Chem.* **2019**, *116*, 282–291, DOI: 10.1016/j.trac.2019.04.023.
- (33) Rolland, A. D.; Biberic, L. S.; Prell, J. S. Investigation of Charge-State-Dependent Compaction of Protein Ions with Native Ion Mobility—Mass Spectrometry and Theory. J. Am. Soc. Mass Spectrom. **2022**, 33 (2), 369–381.
- (34) Zercher, B. P.; Hong, S.; Roush, A. E.; Feng, Y.; Bush, M. F. Are the Gas-Phase Structures of Molecular Elephants Enduring or Ephemeral? Results from Time-Dependent, Tandem Ion Mobility. *Anal. Chem.* **2023**, *95* (25), *9589*–*9597*.
- (35) Breuker, K.; McLafferty, F. W. Stepwise Evolution of Protein Native Structure with Electrospray into the Gas Phase, 10^{-12} to 10^{2} s. *Proc. Natl. Acad. Sci. U.S.A.* **2008**, *105* (47), 18145–18152.
- (36) Hamdy, O. M.; Julian, R. R. Reflections on Charge State Distributions, Protein Structure, and the Mystical Mechanism of Electrospray Ionization. *J. Am. Soc. Mass Spectrom.* **2012**, 23 (1), 1–6.
- (37) Donor, M. T.; Wilson, J. W.; Shepherd, S. O.; Prell, J. S. Lipid Head Group Adduction to Soluble Proteins Follows Gas-Phase Basicity Predictions: Dissociation Barriers and Charge Abstraction. *Int. J. Mass Spectrom.* **2021**, *469*, No. 116670.
- (38) Abi-Ghanem, J.; Rabin, C.; Porrini, M.; Rosu, F.; Gabelica, V. Compaction of RNA Hairpins and Their Kissing Complexes in Native

- Electrospray Mass Spectrometry. J. Am. Soc. Mass Spectrom. 2020, 31 (10), 2035–2043, DOI: 10.26434/chemrxiv.11876505.
- (39) Porrini, M.; Rosu, F.; Rabin, C.; Darré, L.; Gómez, H.; Orozco, M.; Gabelica, V. Compaction of Duplex Nucleic Acids upon Native Electrospray Mass Spectrometry. ACS Cent. Sci. 2017, 3 (5), 454–461
- (40) Reznichenko, O.; Cucchiarini, A.; Gabelica, V.; Granzhan, A. Quadruplex DNA-Guided Ligand Selection from Dynamic Combinatorial Libraries of Acylhydrazones. *Org. Biomol. Chem.* **2021**, *19* (2), 379–386.
- (41) Paul, D.; Marchand, A.; Verga, D.; Teulade-Fichou, M.-P.; Bombard, S.; Rosu, F.; Gabelica, V. Probing Ligand and Cation Binding Sites in G-Quadruplex Nucleic Acids by Mass Spectrometry and Electron Photodetachment Dissociation Sequencing. *Analyst* **2019**, *144* (11), 3518–3524.
- (42) Turner, K. B.; Brinson, R. G.; Yi-Brunozzi, H. Y.; Rausch, J. W.; Miller, J. T.; Le Grice, S. F. J.; Marino, J. P.; Fabris, D. Structural Probing of the HIV-1 Polypurine Tract RNA:DNA Hybrid Using Classic Nucleic Acid Ligands. *Nucleic Acids Res.* **2008**, *36* (8), 2799–2810.
- (43) Paul, D.; Marchand, A.; Verga, D.; Teulade-Fichou, M.-P.; Bombard, S.; Rosu, F.; Gabelica, V. Probing Ligand and Cation Binding Sites in G-Quadruplex Nucleic Acids by Mass Spectrometry and Electron Photodetachment Dissociation Sequencing. *Analyst* **2019**, *144* (11), 3518–3524.
- (44) Turner, K. B.; Brinson, R. G.; Yi-Brunozzi, H. Y.; Rausch, J. W.; Miller, J. T.; Le Grice, S. F. J.; Marino, J. P.; Fabris, D. Structural Probing of the HIV-1 Polypurine Tract RNA:DNA Hybrid Using Classic Nucleic Acid Ligands. *Nucleic Acids Res.* **2008**, *36* (8), 2799–2810, DOI: 10.1093/nar/gkn129.
- (45) Reznichenko, O.; Čucchiarini, A.; Gabelica, V.; Granzhan, A. Quadruplex DNA-Guided Ligand Selection from Dynamic Combinatorial Libraries of Acylhydrazones. *Org. Biomol. Chem.* **2021**, *19* (2), 379–386. 2799–2810. https://doi.org/10.1093/nar/gkn129.
- (46) Heilman-Miller, S. L.; Thirumalai, D.; Woodson, S. A. Role of Counterion Condensation in Folding of the Tetrahymena Ribozyme. I. Equilibrium Stabilization by Cations. *J. Mol. Biol.* **2001**, *306* (5), 1157–1166.
- (47) Lipfert, J.; Doniach, S.; Das, R.; Herschlag, D. Understanding Nucleic Acid—Ion Interactions. *Annu. Rev. Biochem.* **2014**, *83* (1), 813–841.
- (48) Yamagami, R.; Sieg, J. P.; Bevilacqua, P. C. Functional Roles of Chelated Magnesium Ions in RNA Folding and Function. *Biochemistry* **2021**, *60* (31), 2374–2386.
- (49) Strulson, C. A.; Boyer, J. A.; Whitman, E. E.; Bevilacqua, P. C. Molecular Crowders and Cosolutes Promote Folding Cooperativity of RNA under Physiological Ionic Conditions. *RNA* **2014**, 20 (3), 331–347.
- (50) Wilt, H. M.; Yu, P.; Tan, K.; Wang, Y.-X.; Stagno, J. R. FMN riboswitch aptamer symmetry facilitates conformational switching through mutually exclusive coaxial stacking configurations. *J. Struct.Biol.: X* **2020**, *4*, No. 100035.
- (51) Grilley, D.; Soto, A. M.; Draper, D. E. Chapter 3 Direct Quantitation of Mg2+-RNA Interactions by Use of a Fluorescent Dye. *Methods Enzymol.* **2009**, 455, 71–94.
- (52) Daems, E.; Dewaele, D.; Barylyuk, K.; De Wael, K.; Sobott, F. Aptamer-ligand recognition studied by native ion mobility-mass spectrometry. *Talanta* **2021**, 224, No. 121917.
- (53) Misra, V. K.; Draper, D. E. On the role of magnesium ions in RNA stability. *Biopolymers* **1998**, 48 (2–3), 113–135, DOI: 10.1002/(SICI)1097-0282(1998)48:23.0.CO;2-Y.
- (54) Serra, M. J.; Baird, J. D.; Dale, T.; Fey, B. L.; Retatgos, K.; Westhof, E. Effects of Magnesium Ions on the Stabilization of RNA Oligomers of Defined Structures. *RNA* **2002**, *8* (3), 307–323.
- (55) Nobles, K. N. Highly Conserved Modified Nucleosides Influence Mg2+-Dependent TRNA Folding. *Nucleic Acids Res.* **2002**, 30 (21), 4751–4760.
- (56) Saha, A.; Nandi, N. Role of the transfer ribonucleic acid (tRNA) bound magnesium ions in the charging step of amino-

- acylation reaction in the glutamyl tRNA synthetase and the seryl tRNA synthetase bound with cognate tRNA. J. Biomol. Struct. Dyn. **2021**, 40 (18), 8538–8559, DOI: 10.1080/07391102.2021.1914732.
- (57) Holley, R. W.; Apgar, J.; Everett, G. A.; Madison, J. T.; Marquise, M.; Merrill, S. H.; Penswick, J. R.; Zamir, A. Structure of a Ribonucleic Acid. *Science* **1965**, *147* (3664), *1462*–1465.
- (58) Schauss, J.; Kundu, A.; Fingerhut, B. P.; Elsaesser, T. Magnesium Contact Ions Stabilize the Tertiary Structure of Transfer RNA: Electrostatics Mapped by Two-Dimensional Infrared Spectra and Theoretical Simulations. *J. Phys. Chem. B* **2021**, *125* (3), 740–747.
- (59) Suzuki, T.; Nagao, A.; Suzuki, T. Human Mitochondrial TRNAs: Biogenesis, Function, Structural Aspects, and Diseases. *Annu. Rev. Genet.* **2011**, 45 (1), 299–329.
- (60) D'Souza, A. R.; Minczuk, M. Mitochondrial Transcription and Translation: Overview. *Essays Biochem.* **2018**, 62 (3), 309–320, DOI: 10.1042/ebc20170102.
- (61) Yarham, J. W.; Elson, J. L.; Blakely, E. L.; McFarland, R.; Taylor, R. W. Mitochondrial TRNA Mutations and Disease. *Wiley Interdiscip. Rev.: RNA* **2010**, *1* (2), 304–324, DOI: 10.1002/wrna.27.
- (62) Tuppen, H. A. L.; Blakely, E. L.; Turnbull, D. M.; Taylor, R. W. Mitochondrial DNA Mutations and Human Disease. *Biochim. Biophys. Acta, Bioenerg.* **2010**, *1797* (2), 113–128, DOI: 10.1016/j.bba-bio.2009.09.005.
- (63) Thornlow, B. P.; Hough, J.; Roger, J. M.; Gong, H.; Lowe, T. M.; Corbett-Detig, R. B. Transfer RNA genes experience exceptionally elevated mutation rates. *Proc. Natl. Acad. Sci. U.S.A.* **2018**, *115* (36), 8996–9001, DOI: 10.1101/229906.
- (64) Sheng, B.; Fong, M. K.; Kwan Ng, W.; Lam Chen, S. P.; Miu Mak, C. MELAS, MIDD and Beyond: M.3243A > G MT-TL1Mutation in Adult Patients. *Int. J. Clin. Med.* **2016**, 07 (07), 487–495
- (65) Lin, D.-S.; Huang, Y.-W.; Ho, C.-S.; Huang, T.-S.; Lee, T.-H.; Wu, T.-Y.; Huang, Z.-D.; Wang, T.-J. Impact of Mitochondrial A3243G Heteroplasmy on Mitochondrial Bioenergetics and Dynamics of Directly Reprogrammed MELAS Neurons. *Cells* **2023**, *12* (1), 15.
- (66) Liu, X.; Wu, N.; Shanmuganathan, A.; Klemm, B. P.; Howard, M. J.; Lim, W. H.; Koutmos, M.; Fierke, C. A. Kinetic mechanism of human mitochondrial RNase P. *bioRxiv* **2019**, 666792 DOI: 10.1101/666792.
- (67) Karasik, A.; Wilhelm, C. A.; Fierke, C. A.; Koutmos, M. Disease-associated mutations in mitochondrial precursor tRNAs affect binding, m1R9 methylation, and tRNA processing by mtRNase P. RNA 2020, 27 (4), 420–432, DOI: 10.1101/2020.07.07.191726.
- (68) Wittenhagen, L. M.; Kelley, S. O. Dimerization of a Pathogenic Human Mitochondrial TRNA. *Nat. Struct. Biol.* **2002**, *9* (8), 586–590, DOI: 10.1038/nsb820.
- (69) Machnicka, M. A.; Olchowik, A.; Grosjean, H.; Bujnicki, J. M. Distribution and Frequencies of Post-Transcriptional Modifications in TRNAs. *RNA Biol.* **2014**, *11* (12), 1619–1629.
- (70) Suzuki, T.; Suzuki, T. A Complete Landscape of Post-Transcriptional Modifications in Mammalian Mitochondrial TRNAs. *Nucleic Acids Res.* **2014**, *42* (11), 7346–7357.